CALCULATION MODEL FOR THE INDUCED VOLTAGE IN RECTANGULAR COILS ABOVE CONDUCTIVE PLATES

Siquan Zhang[1], Nathan Ida[2]

[1]Department of Electrical and Automation, Shanghai Maritime University, Shanghai, 201306, China
[2]Department of Electrical and Computer Engineering, The University of Akron, Akron, OH, 44325-3904, USA

Abstract. *Electromagnetic NDT methods and in particular eddy currents play an important role in nondestructive testing of conducting materials. In testing conductive structures, rectangular coils are often more useful than circular coils. A particular configuration consists of two rectangular coils located above the conductive plates, one placed parallel to the plates serving as an excitation coil and the other perpendicular to the plates serving as a sensing coil. In this work we derive analytical expressions for the induced voltage variations in the pick-up coil. Then the influences of the plate thickness, the exciting frequency and the moving speed of the conductor on the induced voltage variation are analyzed. The analytical calculation results are verified using the finite element method.*

Key words: *Eddy current testing, Conductive plates, Rectangular coil, Induced voltage, Finite element method.*

1. INTRODUCTION

Eddy current testing (ECT) techniques are widely used in testing of conductive structures with advantages of high sensitivity when testing for surface flaws [1-3]. In standard eddy current testing a circular coil carrying current is used to test the conductive specimen. The alternating current in the coil generates an alternating magnetic field, which interacts with the test specimen and generates eddy currents. However, rectangular coils are more useful than circular coils, because the rectangular coil is not axisymmetric, hence it affects the field inside the medium resulting in higher sensitivity to sub-surface flaws [4]. In spite of these advantages, rectangular coils have been seldom discussed in the literature. In this paper, we analyse a model with two rectangular coils, one serving as the exciting coil and the other is the pick-up coil, both located above the conductive plates. The conductive materials' characteristics or parameters of flaws can be evaluated

from the induced voltage variation in the pick-up coil. The validity of the theoretical analysis is confirmed by the finite element method (FEM).

2. THEORETICAL ANALYSIS

2.1. Analytical model

Fig. 1 shows two rectangular single-turn coils located above multi-layer conductive plates. The exciting coil is parallel to the surface of the conductor which coincides with the $z = 0$ plane. The dimensions of the exciting coil are $2a_1$, $2b_1$ and a lift-off z_0. An AC harmonic current $Ie^{j\omega t}$ flows in the coil. The pick-up coil is parallel to the yz plane and perpendicular to the conductor, it has dimensions of $2a_2$, $2b_2$ and a lift-off z_0+w_2. The thickness, conductivity and permeability of the two layer conductive plate are assumed to be d_i, σ_i and μ_i ($i = 1, 2$) and the conductive media are assumed to be linear, isotropic and homogeneous.
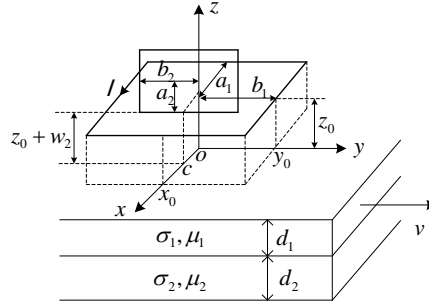
Fig. 1 Filamentary rectangular coils above a multi-layer conductor

To simplify the analysis, the solution region is divided into region 0, 1 and 2. In Region 0 ($z > 0$), the incident magnetic flux density B_i generated by the exciting current and the reflected magnetic flux density B_r generated by inducted eddy currents exist simultaneously. The incident magnetic flux density B_i can be expressed by the vector potential A_i as:

$$\nabla \times \nabla \times A_i = \mu_0 J \tag{1}$$

$$B_i = \nabla \times A_i \tag{2}$$

The reflected magnetic flux density B_r satisfies the following:

$$\nabla \times B_r = 0 \tag{3}$$

$$\nabla^2 B_r = 0 \tag{4}$$

Region 1 ($-d < z < 0$) is the top conductive plate. The magnetic flux density B_1 in this region satisfies the following:

$$\nabla^2 B_1 - \sigma_1 \mu_1 v \frac{\partial B_1}{\partial y} - j\omega\sigma_1\mu_1 B_1 = 0 \tag{5}$$

$$\nabla \cdot B_1 = 0 \tag{6}$$

Region 2 $(z < -d)$ is the lower conductive plate. The magnetic flux density B_2 in this region satisfies:

$$\nabla^2 B_2 - \sigma_2 \mu_2 v \frac{\partial B_2}{\partial y} - j\omega\sigma_2\mu_2 B_2 = 0 \tag{7}$$

$$\nabla \cdot B_2 = 0 \tag{8}$$

To solve these equations, the double Fourier transform and its inverse are introduced:

$$b(\xi, \eta, z) = \int_{-\infty}^{\infty} \int_{-\infty}^{\infty} B(x, y, z) \cdot e^{j(x\xi + y\eta)} dx dy \tag{9}$$

$$B(x, y, z) = \frac{1}{4\pi^2} \int_{-\infty}^{\infty} \int_{-\infty}^{\infty} b(\xi, \eta, z) \cdot e^{-j(x\xi + y\eta)} d\xi d\eta \tag{10}$$

where ξ and η are the integration variables.

2.2. Incident magnetic flux density

The single filamentary rectangular coil consists of four finite length wires, as shown in Fig.1. By solving (1), the vector potential generated at an arbitrary point $p(x, y, z)$ by a source point (x', y', z') in the coil can be written as:

$$A(x, y, z) = \frac{\mu_0}{4\pi} \int_v \frac{J(x', y', z') dv'}{R} \tag{11}$$

where J is the current density in the coil, v is the coil segment carrying current, R is the distance of $p(x, y, z)$ to the source point (x', y', z') as follow:

$$R = \sqrt{(x - x')^2 + (y - y')^2 + (z - z')^2} \tag{12}$$

Performing the Fourier transform on (11), the expression of the vector potential in the region $z < z_0$ is obtained as:

$$
\begin{aligned}
a(\xi, \eta, z) &= \frac{\mu_0}{4\pi} \int_v J(x', y', z') \cdot \{\int_{-\infty}^{\infty} \int_{-\infty}^{\infty} \frac{1}{R} \cdot e^{j(x\xi + y\eta)} dx dy\} dv' \\
&= \frac{\mu_0}{2} \int_v J(x', y', z') e^{j(\xi x' + \eta y')} \frac{1}{\sqrt{\xi^2 + \eta^2}} e^{-|z - z_0|\sqrt{\xi^2 + \eta^2}} dv'
\end{aligned}
\tag{13}
$$

Similarly, the components of the incident magnetic flux density are obtained by performing the Fourier transform on (2):

$$b_x = -j\eta a_z - \frac{\partial a_y}{\partial z}, \quad b_y = \frac{\partial a_x}{\partial z} + j\xi a_z, \quad b_z = -j\xi \cdot a_y + j\eta \cdot a_x \tag{14}$$

As shown in Fig. 1, the wire parallel to the x axis satisfies $J(x', y', z') = I$, $y' = y_0$ and $z - z_0 < 0$. Substituting these into (13), the x component of the vector potential becomes:

$$
\begin{aligned}
a_x &= \frac{\mu_0}{2} \int_v J(x', y', z') e^{j(\xi x' + \eta y')} \frac{1}{\sqrt{\xi^2 + \eta^2}} e^{-|z - z_0|\sqrt{\xi^2 + \eta^2}} dv' = \frac{\mu_0 I}{2} \frac{e^{(z - z_0)\sqrt{\xi^2 + \eta^2}}}{\sqrt{\xi^2 + \eta^2}} e^{j\eta y_0} \int_{-x_0}^{x_0} e^{j\xi x'} dx' \\
&= \frac{\mu_0 I}{2} \frac{e^{(z - z_0)\sqrt{\xi^2 + \eta^2}}}{\sqrt{\xi^2 + \eta^2}} e^{j\eta y_0} \frac{2\sin(\xi x_0)}{\xi} = \frac{\mu_0 I \sin(\xi x_0) e^{j\eta y_0} e^{(z - z_0)\sqrt{\xi^2 + \eta^2}}}{\xi\sqrt{\xi^2 + \eta^2}}
\end{aligned}
\tag{15}
$$

Similarly, the wire parallel to the y axis satisfies $J(x', y', z') = I$, $x' = x_0$ and $z - z_0 < 0$, substituting into (13), the y components of the vector potential becomes:

$$a_y = \frac{\mu_0}{2} \int_v J(x', y', z') e^{j(\xi x' + \eta y')} \frac{1}{\sqrt{\xi^2 + \eta^2}} e^{-|z-z_0|\sqrt{\xi^2+\eta^2}} dv' = \frac{\mu_0 I}{2} \frac{e^{(z-z_0)\sqrt{\xi^2+\eta^2}}}{\sqrt{\xi^2 + \eta^2}} e^{j\xi x_0} \int_{-y_0}^{y_0} e^{j\eta y'} dy'$$

$$= \frac{\mu_0 I}{2} \frac{e^{(z-z_0)\sqrt{\xi^2+\eta^2}}}{\sqrt{\xi^2 + \eta^2}} e^{j\xi x_0} \frac{2\sin(\eta y_0)}{\eta} = \frac{\mu_0 I \sin(\eta y_0) e^{(z-z_0)\sqrt{\xi^2+\eta^2}}}{\eta \sqrt{\xi^2 + \eta^2}} e^{j\xi x_0} \qquad (16)$$

The x components of the magnetic flux density can be obtained by substituting (15) and (16) into (14) as follows:

$$b_{ix} = -\frac{\partial a_{1y}}{\partial z} = -\frac{\partial}{\partial z} \{a_{2y}(a_1, b_1, z_0) - a_{2y}(-a_1, b_1, z_0)\} = -\frac{j2\mu_0 I \sin(a_1\xi)\sin(b_1\eta)}{\eta} \cdot e^{(z-z_0)\sqrt{\xi^2+\eta^2}} \quad (17)$$

Similarly, the y and z components of the magnetic flux density can be obtained as:

$$b_{iy} = -\frac{j2\mu_0 I \sin(a_1\xi)\sin(b_1\eta)}{\xi} e^{(z-z_0)\sqrt{\xi^2+\eta^2}} \qquad (18)$$

$$b_{iz} = \frac{2\mu_0 I \sqrt{\xi^2 + \eta^2} \sin(a_1\xi)\sin(b_1\eta)}{\xi\eta} e^{(z-z_0)\sqrt{\xi^2+\eta^2}} \qquad (19)$$

The general solution for the z component of the incident magnetic flux density in region 0 is:

$$b_{iz} = C_{iz} e^{z\sqrt{\xi^2+\eta^2}} \qquad (20)$$

where the coefficients C_{iz} are:

$$C_{iz} = \frac{2\mu_0 I \sqrt{\xi^2 + \eta^2} \sin(a_1\xi)\sin(b_1\eta)}{\xi\eta} e^{-z_0\sqrt{\xi^2+\eta^2}} \qquad (21)$$

2.3. Reflected magnetic flux density

Performing the Fourier transform on (4), the reflected magnetic flux density in region 0 can be expressed as:

$$\frac{\partial^2 b_r}{\partial z^2} - (\xi^2 + \eta^2)b_r = 0 \qquad (22)$$

In similar fashion, performing the Fourier transform on (5) and (7), the magnetic flux density in region 1 and 2 can be expressed as:

$$\frac{\partial^2 b_1}{\partial z^2} - (\xi^2 + \eta^2 - j\sigma_1\mu_1 v\eta + j\omega\sigma_1\mu_1)b_1 = 0 \qquad (23)$$

$$\frac{\partial^2 b_2}{\partial z^2} - (\xi^2 + \eta^2 - j\sigma_2\mu_2 v\eta + j\omega\sigma_2\mu_2)b_2 = 0 \qquad (24)$$

The normal component of B and the tangential components of H must be continuous on the $z = 0$ and $z = -d$ planes.

Applying the continuity of B_z, we obtain

$$b_{iz} + b_{rz} = b_{1z} \quad (z = 0) \tag{25}$$

$$b_{1z} = b_{2z} \quad (z = -d) \tag{26}$$

Applying the continuity of H_x, we obtain

$$\frac{(b_{ix} + b_{rx})}{\mu_0} = \frac{b_{1x}}{\mu_1} \quad (z = 0) \tag{27}$$

$$\frac{b_{1x}}{\mu_1} = \frac{b_{2x}}{\mu_2} \quad (z = -d) \tag{28}$$

Applying the continuity of H_y, we obtain

$$\frac{(b_{iy} + b_{ry})}{\mu_0} = \frac{b_{1y}}{\mu_1} \quad (z = 0) \tag{29}$$

Due to the fact that $\nabla \cdot J = 0$, the current density J_z does not exist in regions 1 and 2, and we get:

$$\xi b_{1y} = \eta b_{1x} \tag{30}$$

$$\xi b_{2y} = \eta b_{2x} \tag{31}$$

The following equations are obtained from (3)

$$-j\eta b_{rz} = \frac{\partial b_{ry}}{\partial z} \tag{32}$$

$$-j\xi b_{rz} = \frac{\partial b_{rx}}{\partial z} \tag{33}$$

Following similar steps, the following equations are obtained from (6) and (8):

$$-j\xi b_{1x} - j\eta b_{1y} + \frac{\partial b_{1z}}{\partial z} = 0 \tag{34}$$

$$-j\xi b_{2x} - j\eta b_{2y} + \frac{\partial b_{2z}}{\partial z} = 0 \tag{35}$$

The coefficient of the reflected magnetic flux density is obtained by solving the above equations:

$$D_{rz} = \frac{(n+1) + (1-n)Pe^{2\gamma_1 d}}{1-n+(1+n)Pe^{2\gamma_1 d}} C_{iz} \tag{36}$$

where

$$\xi = \varsigma \cos\varphi, \ \eta = \varsigma \sin\varphi, \ \varsigma = \sqrt{\xi^2 + \eta^2}, \ \frac{\mu_1 \varsigma}{\mu_2 \gamma_1} = m, \ \frac{1+m}{1-m} = P, \ \frac{\mu_0 \gamma_1}{\mu_1 \varsigma} = n,$$

$$\gamma_1 = \sqrt{\xi^2 + \eta^2 - j\sigma_1\mu_1 v\eta + j\omega\sigma_1\mu_1} \tag{37}$$

Let

$$\frac{(n+1) + (1-n)Pe^{2\gamma_1 d}}{1-n+(1+n)Pe^{2\gamma_1 d}} = \kappa \tag{38}$$

The coefficient of the reflected magnetic flux density becomes:

$$D_{rz} = \frac{2\mu_0 I\kappa\sqrt{\xi^2+\eta^2}\,\sin(a_1\xi)\sin(b_1\eta)\cdot e^{-z_0\sqrt{\xi^2+\eta^2}}}{\xi\eta} \tag{39}$$

$$D_{rx} = \frac{j\xi}{\sqrt{\xi^2+\eta^2}}\cdot D_{rz} = \frac{2j\mu_0 I\kappa\cdot\sin(a_1\xi)\cdot\sin(b_1\eta)\cdot e^{-z_0\sqrt{\xi^2+\eta^2}}}{\eta} \tag{40}$$

The x component of the reflected magnetic flux density becomes:

$$b_{rx} = D_{rx}e^{-z\sqrt{\xi^2+\eta^2}} = \frac{2j\mu_0 I\kappa\sin(a_1\xi)\sin(b_1\eta)\cdot e^{-(z+z_0)\sqrt{\xi^2+\eta^2}}}{\eta} \tag{41}$$

The x component of the reflected magnetic flux density in region 0 is obtained by performing the inverse Fourier transform on (41):

$$B_{rx} = \frac{j\mu_0 I}{2\pi^2}\int_{-\infty}^{\infty}\int_{-\infty}^{\infty}\frac{\sin(a_1\xi)\sin(b_1\eta)}{\eta}\,\kappa\cdot e^{-(z+z_0)\varsigma}\,e^{-j(x\xi+y\eta)}d\xi d\eta \tag{42}$$

Fig. 2 shows two multi-turn rectangular coils obtained by extending the two single-turn coils shown in Fig. 1 in width and length respectively. The coil parallel to the surface of the conductor is the excitation coil and the coil perpendicular to the conductor is the pick-up coil. The turns of the excitation and pick-up coil are N_1 and N_2 respectively. The lower surfaces of the two rectangular coils are level with each other.
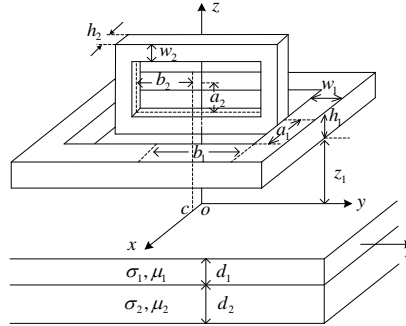
Fig. 2 Configuration of two multi-turn rectangular coils

The reflected magnetic flux density generated by the multi-turn rectangular exciting coil shown in Fig. 2 is obtained by integrating (42) with respect to the width and length as follows:

$$\begin{aligned}
B_{rx}^{total} &= \frac{N_1}{w_1 h_1}\int_{z_1}^{z_1+h_1}dz_0\int_0^{w_1}B_{rx}dp = \frac{j\mu_0 IN_1}{2\pi^2 w_1 h_1}\int_{-\infty}^{\infty}\int_{-\infty}^{\infty}\frac{\kappa}{\eta}\,\{\int_0^{w_1}\sin[(a_1+p)\xi)]\sin[(b_1+p)\eta]dp\} \\
&\quad \cdot\{\int_{z_1}^{z_1+h_1}e^{-z_0\varsigma}dz_0\}\cdot e^{-z\varsigma}\cdot e^{-j(x\xi+y\eta)}d\xi d\eta \\
&= \frac{j\mu_0 IN_1}{2\pi^2 w_1 h_1}\int_{-\infty}^{\infty}\int_{-\infty}^{\infty}\frac{\kappa\cdot k_1}{\eta\varsigma}\cdot[e^{-\varsigma(z+z_1)}-e^{-\varsigma(z+z_1+h_1)}]\cdot e^{-j(x\xi+y\eta)}d\xi d\eta
\end{aligned} \tag{43}$$

where

$$\int_{z_1}^{z_1+h_1} e^{-z_0\varsigma} dz_0 = \frac{1}{\varsigma}[e^{-z_1\varsigma} - e^{-(z_1+h_1)\varsigma}] \tag{44}$$

$$k_1 = \int_0^{w_1} \sin[(a_1 + p)\xi)]\sin[(b_1 + p)\eta]dp$$

$$= \frac{\sin[a_1\xi - b_1\eta + (\xi - \eta)w_1] - \sin(a_1\xi - b_1\eta)}{2(\xi - \eta)} + \frac{\sin(a_1\xi + b_1\eta) - \sin[a_1\xi + b_1\eta + (\xi + \eta)w_1]}{2(\xi + \eta)} \tag{45}$$

Fig. 3 shows a comparison of the variation of the reflected magnetic flux density's x component as calculated from (43) and as simulated using Maxwell 3D respectively. The results of the simulation are obtained by subtracting the x component of the magnetic flux density without the conductor from the x component of the magnetic flux density with the conductor. The points shown belong to the line between (-16,0,5) and (16,0,5) which is located below the exciting coil and above the conductive plate. It can be seen that the analytical calculation results agree with the simulated results very well.
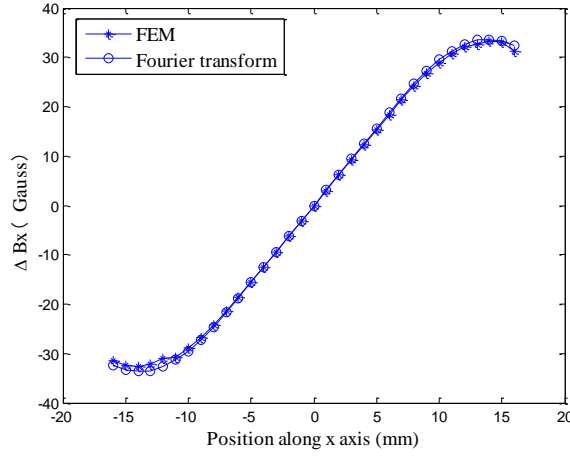
Fig. 3 Variations of the x component the magnetic flux density
calculated from the analytical and FEM simulation

3. INDUCED VOLTAGE IN PICKUP COIL

3.1. Magnetic flux penetrating through the pick-up coil

To obtain the reflected magnetic flux penetrating through the multi-turn rectangular pickup coil shown in Fig. 2, we first derive the reflected magnetic flux penetrating through the single-turn rectangular coil with lengths $2a_2$, $2b_2$, and assume it is located at $(c, 0, z_c)$, where $z_c = z_1 + w_2 + a_2$. The reflected magnetic flux penetrating through the single-turn coil is obtained by integrating (43) on the area of coil as:

$$\phi_r = \int_{z_c-a_2}^{z_c+a_2} dz \int_{-b_2}^{b_2} B_{rx}^{total}\Big|_{x=c} dy =$$

$$= \frac{j\mu_0 IN_1}{2\pi^2 w_1 h_1} \int_{-\infty}^{\infty}\int_{-\infty}^{\infty} \frac{\kappa k_1}{\eta \varsigma} e^{-j\xi c} [e^{-z_1\varsigma} - e^{-(z_1+h_1)\varsigma}] \cdot \{\int_{z_c-a_2}^{z_c+a_2} e^{-z\varsigma}dz\} \{\int_{-b_2}^{b_2} e^{-jy\eta}dy\}d\xi d\eta$$

$$= \frac{j\mu_0 IN_1}{\pi^2 w_1 h_1} \int_{-\infty}^{\infty}\int_{-\infty}^{\infty} \frac{\kappa k_1}{\eta^2\varsigma^2} [e^{-z_1\varsigma} - e^{-(z_1+h_1)\varsigma}] e^{-\varsigma z_c} \cdot e^{-j\xi c} \cdot [e^{\varsigma a_2} - e^{-\varsigma a_2}] \sin(\eta b_2)\, d\xi d\eta \quad (46)$$

Then the reflected magnetic flux penetrating through the multi-turn rectangular pickup coil is obtained by integrating (46) with respect to the width and length of pickup coil as follows:

$$\phi = \frac{N_2}{w_2 h_2} \int_0^{w_2} dp \int_{c-h_2/2}^{c+h_2/2} \phi_r dc = \frac{j\mu_0 IN_1 N_2}{\pi^2 w_1 h_1 w_2 h_2} \int_{-\infty}^{\infty}\int_{-\infty}^{\infty} \frac{\kappa k_1}{\eta^2\varsigma^2} [e^{-(z_1+z_c)\varsigma} - e^{-(z_1+z_c+h_1)\varsigma}]$$

$$\cdot \{\int_{c-h_2/2}^{c+h_2/2} e^{-j\xi c}dc\} \{\int_0^{w_2} [e^{\varsigma(a_2+p)} - e^{-\varsigma(a_2+p)}] \sin[\eta(b_2+p)]dp\}d\xi d\eta$$

$$= \frac{j2\mu_0 IN_1 N_2}{\pi^2 w_1 h_1 w_2 h_2} \int_{-\infty}^{\infty}\int_{-\infty}^{\infty} \frac{\kappa k_1 k_2}{\eta^2 \xi \varsigma^2} \sin(\frac{h_2}{2}\xi) \cdot e^{-j\xi c} \cdot [e^{-(2z_1+w_2+a_2)\varsigma} - e^{-(2z_1+w_2+a_2+h_1)\varsigma}]d\xi d\eta \quad (47)$$

where

$$k_2 = \int_0^{w_2} [e^{\varsigma(a_2+p)} - e^{-\varsigma(a_2+p)}]\sin[\eta(b_2+p)]dp$$

$$= \frac{\varsigma \sin\eta(b_2+w_2)[e^{\varsigma(w_2+a_2)} + e^{-\varsigma(w_2+a_2)}] - \eta\cos\eta(b_2+w_2)[e^{\varsigma(w_2+a_2)} - e^{-\varsigma(w_2+a_2)}]}{\eta^2 + \varsigma^2}$$

$$+ \frac{\eta\cos(\eta b_2)[e^{\varsigma a_2} - e^{-\varsigma a_2}] - \varsigma\sin(\eta b_2)[e^{\varsigma a_2} + e^{-\varsigma a_2}]}{\eta^2 + \varsigma^2} \quad (48)$$

3.2. Induced voltage in the rectangular pickup coil

The relationship between the magnetic flux penetrating through the pickup coil and induced voltage is:

$$V = -\frac{d\phi}{dt} = -j\omega\phi \quad (49)$$

Therefore, the induced voltage can be derived as:

$$V = \frac{2\omega\mu_0 IN_1 N_2}{\pi^2 w_1 h_1 w_2 h_2} \int_{-\infty}^{\infty}\int_{-\infty}^{\infty} \frac{\kappa k_1 k_2}{\eta^2 \xi \varsigma^2} \sin(\frac{h_2\xi}{2}) \cdot e^{-j\xi c} \cdot [e^{-(2z_1+w_2+a_2)\varsigma} - e^{-(2z_1+w_2+a_2+h_1)\varsigma}]d\xi d\eta \quad (50)$$

4. RESULTS

The induced voltage variation of the rectangular pick-up coil is now calculated by considering the influencing factors based on the expressions derived in the previous section. The parameters of the coils and the conductive plates are given in Tables 1 and 2 respectively.

Table 1 Parameters of the rectangular coil

Exciting coil		Pick-up coil	
a_1 (mm)	12	a_2 (mm)	3
b_1 (mm)	12	b_2 (mm)	5
z_1 (mm)	1	z_1 (mm)	1
w_1 (mm)	2	w_2 (mm)	5
h_1 (mm)	8	h_2 (mm)	2
turns	500	c (mm)	6
		turns	300

Table 2 Parameters of the conductive plate

Top layer	σ_1 (S/m)	3.8×10^7
	μ_{r1}	1
Lower layer	σ_2 (S/m)	5.8×10^7
	μ_{r2}	1

Fig. 4 shows the induced voltage due to the conductive plates as a function of the excitation frequency. The thickness of the top-layer conductor is 200 μm and the thickness of the lower-layer is semi-infinite and both conductors are stationary. c is the distance from the center of the pick-up coil to the z axis. It can be seen from Fig. 4 that the variation of the induced voltage increases with frequency. At any given exciting frequency, the pick-up coil with larger distance to the z axis has a higher induced voltage.
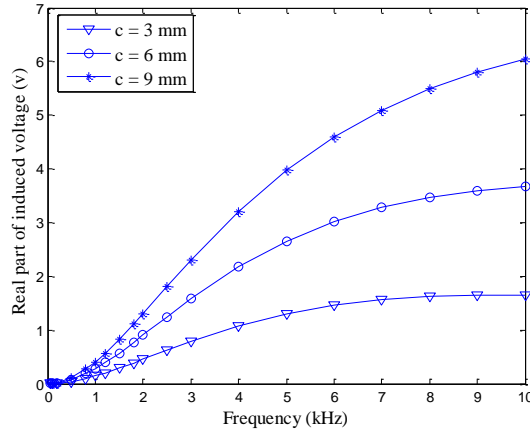
Fig. 4 Induced voltage in the pickup coil as a function of exciting frequency

Fig. 5 compares the induced voltage calculated from the analytical method and FEM simulation. The analytical results are calculated as the square root of the sum of squares of the real and imaginary parts of the induced voltage. The results of the FEM are the effective values of the induced voltage obtained in pick-up coil, simulated with a time-dependent formulation.
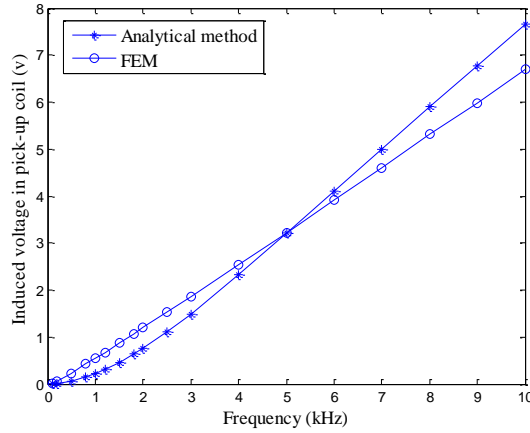
Fig. 5 Comparation of the induced voltage variation in rectangular pick-up coil
from analytical and FEM at different excitation frequency

The induced voltages in the coil for different thicknesses of the top-layer conductor are shown in Fig. 6. The excitation frequencies are fixed at 0.5, 2, and 5 kHz respectively, and the conductor is stationary. The distance from the center of the pick-up coil to the z axis is fixed at 9 mm. The induced voltage variation initially increases with the thickness, then, at a specific thickness, the induced voltage reaches a maximum, followed by a decreases with increasing thickness. As can be seen from Fig. 6, the higher excitation frequency produces a higher maximum at a smaller thickness, but the induced voltage decreases faster with increasing excitation frequency.
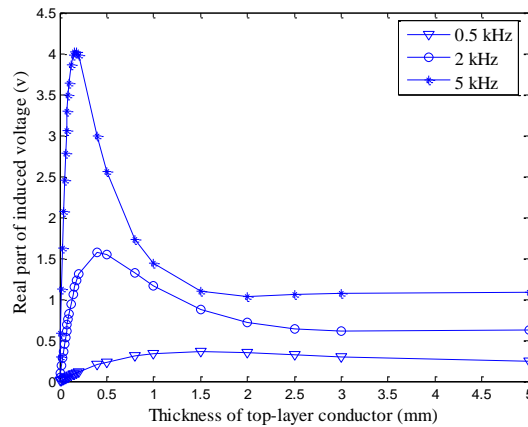
Fig. 6 Induced voltage in pickup coil as a function of top-layer conductor thickness

The speed characteristics are shown in Fig. 7. The induced voltage variations are calculated at speeds from $v = 0$ to 50 m/s. The excitation frequency is fixed at 2 kHz. Fig. 7 shows the differences of the coils induced voltage at different speeds of the conductor relative to the

coils' induced voltage when the conductor is stationary. The rectangular coils' induced voltage variation keeps increasing with the moving speed of conductor, the maximum variation of induced voltage is achieved with the top-layer conductor of thickness 200 μm.
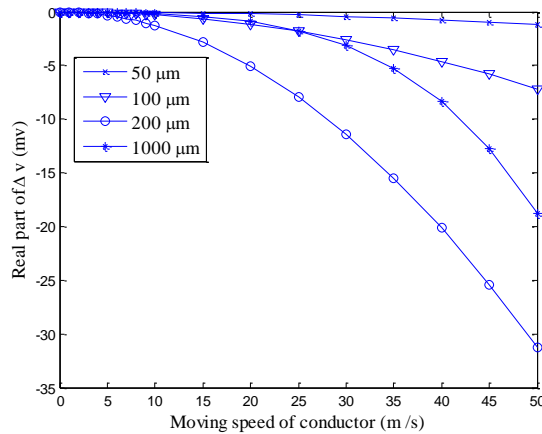
Fig. 7 Induced voltage of pickup coil at different speed of conductor

5. CONCLUSION

A closed-form expression for the induced voltage between a pair of rectangular coils above a multi-layered conductive plate has been derived using a 2D Fourier transform method. The excitation coil is parallel to the plates and the pickup coil is perpendicular to the conductor. We discussed the influencing factors on the induced voltage, such as the excitation frequency, the thickness of the top-layer conductor and the speed of the conductor. The calculation model and results can be extended and used in the forward model of quantitative detection for eddy current testing of multi-layer conductive structures.

REFERENCES

[1] T. Theodoulidis, N. Poulakis, A. Dragogias, "Rapid computation of eddy current signals from narrow cracks", *NDT&E International*, vol. 43, pp. 13-19, 2010.

[2] L. Guohou, H. Pingjie, C. Peihua, "Quantitative nondestructive estimation of deep defects in conductive structures", *International Journal of Applied Electromagnetics and Mechanics*, vol. 33 (3-4), pp. 1273-1278, 2010.

[3] J.W. Luquire, W.E. Deeds, C.V. Dodd, "Alternating Current Distribution Between Planar Conductors", *Journal of Applied Physics*, vol.41 (10), pp. 3983-3991, 1970.

[4] T.P. Theodoulidis, E.E. Kriezis, "Impedance evaluation of rectangular coils for eddy current testing of planar media", *NDT & E International*, vol. 35(6), pp. 407-414, 2002.

[5] Y. Lei, X. Ma, "Calculation of Impedance in an Eddy-Current Coil by Numerical Integration Method", *Transactions of China Electrotechnical Society*, vol. 11 (1), pp. 17-20, 1996.

[6]   P. Huang, Z. Wu, J. Zheng, "Inversion Algorithms for Multi-layered Thickness Measurement in Eddy Current Testing", Chinese Journal of Scientific Instrument, vol. 26 (4), pp. 428-432, 2005.

[7]   T. Theodoulidis, E. Kriezis, "Series expansions in eddy current nondestructive evaluation models", *Journal of Materials Processing Technology*, vol. 161 (5), 2005.

[8]   C.V. Dodd, W.E. Deeds, "Analytical solutions to eddy current probe-coil problems", *Journal of applied physics*, vol. 39 (6), 2829-2838, 1968.

[9]   Y.U. Yating, D.U. Ping an, L.I. Daisheng, "Computational Methods of Coil Impedance of Eddy Current Sensor", *Chinese Journal of Mechanical Engineering*, vol. 43 (2), pp. 210-214, 2007.

[10] J.-L. Ren, H.-B. Diao, J.-H. Tang, "Simulation of the Lift-off Effect of Eddy Current Testing Based on ANSYS", *Chinese Journal of Sensors and Actuation*, vol. 21 (6), pp. 967-971, 2008.